REPORT No. 367

PRESSURE DISTRIBUTION OVER A THICK, TAPERED AND TWISTED MONOPLANE WING MODEL—N. A. C. A. 81–J

By Carl J. Wenzinger

SUMMARY

This report presents the results of pressure distribution tests on a thick, tapered and twisted monoplane wing model. The investigation was conducted for the purpose of obtaining data on the aerodynamic characteristics of the new wing and to provide additional information suitable for use in the design of tapered cantilever wings. The tests included angles of attack up to 90 degrees and were made in the Atmospheric Wind Tunnel of the National Advisory Committee for Aeronautics.

The span loading over the wing was approximately of elliptical shape, which gave rise to relatively small bending moments about the root. The angle of zero lift for all sections along the span varied only within ±0.4 degree of the angle of zero lift for the whole wing, resulting in small leading edge loads for the high-speed condition of flight. The results also add to the available information for the study of stability at large angles of attack.

INTRODUCTION

The structural design of airplane wings calls for a knowledge of the manner in which the air loads are distributed over the wing as well as the magnitude of the total loads. Standard load distributions, for example, such as are specified by the Department of Commerce, are only approximate, and while wings designed according to these loadings may be generally safe, they are doubtless often heavier than need be. It is, therefore, desirable to know more exactly the actual load distribution over a given type of wing if minimum weight is to be obtained.

The increasing amount of interest in cantilever monoplane wing systems has furnished the basis for an extensive pressure distribution investigation made in the Atmospheric Wind Tunnel of the National Advisory Committee for Aeronautics. Several models of tapered wings suitable for internal bracing have previously been tested and the results published (Reference 1). The results of these tests indicated that further improvement in aerodynamic and geometric features were desirable, and in consequence, a new tapered wing was designed.

It was desired to produce a wing having the following characteristics:

1. Relatively small bending moments at the wing root.
2. Equal length spars.
3. Reduced leading edge loads, for the nose dive condition.
4. High maximum lift.
5. Minimum induced drag for any given lift and aspect ratio.

This new wing, designated as the N. A. C. A. 81–J (see fig. 1), was developed from the following considerations:

A linear taper having a ratio of tip to root of 0.5, in plan form, provides for approximately elliptical span loading, and causes the lateral center of pressure to move nearer to the center of the span, thereby giving relatively small bending moments about the wing root.

The wing tip was shaped so as to provide for good load distribution and to enable the use of spars of equal length.

In order to reduce the loads on the leading edge of the wing, particularly in the nose dive condition of flight, the wing was to be given a geometric washin so that all sections along the span would be at zero lift simultaneously. If the sections also stalled at approximately the same angle of attack, then a maximum over-all lift would probably be attained as well.

High maximum lift was further assured by making the wing root and tip profiles of the Joukowski type, which profiles were developed by the method given in Reference 2. These profiles were slightly modified, however, by thickening the trailing edges somewhat.

The elliptical span loading previously referred to is also the theoretical condition for minimum drag of the wing, so that from a consideration of the foregoing, it can be seen that probably a good compromise would be effected in obtaining a wing with the desired characteristics.

Preliminary tests on a model of the new wing indicated an insufficient amount of twist had been provided at the tips to satisfy the zero lift conditions. A second model was, therefore, built with a greater geometric washin, but otherwise the same as the first model. The results of pressure distribution tests on this latter model of the new wing are presented in this report for angles of attack up to 90°. These

results add to the available information for the design of tapered monoplane wings, and for the study of stability at large angles of attack.

Attention is invited to the difference between the aerodynamic and the geometric washin. The present wing at zero lift has a fairly large geometric washin which corresponds, however, to zero aerodynamic washin.

MODEL AND APPARATUS

The airfoil used in these tests was a half-span model, and was tapered in thickness and plan form, with a geometric wash-in at the tip of 6° 45′. (See fig. 1.) It was constructed of laminated mahogany, the ordinates being held accurate to within ± 0.01 inch of those specified in Table I. The tip was first made straight, and then carefully shaped to the dimensions shown.

For purposes of pressure distribution testing, 37 pairs of small brass tubes were built into the airfoil, one tube of each pair opening as an orifice in the upper surface, and the other tube opening in the lower surface. The tubes extended down through the wing butt and terminated in small brass nipples. Six tubes were found to be defective after testing for leaks and these are indicated on Figure 1. The pressures indicated by them were not used, but the values of pressure heads have been interpolated at these locations. Orifice locations around the profile and the spacing of the orifice groups along the span are shown in Figure 1, and given in Table II.

The tests were made in the Atmospheric Wind Tunnel (Reference 3), on the half-span model mounted vertically on a horizontal "separation" plane, the assumption being made that the imaginary plane of symmetry of a wing can be replaced by an actual plane surface without changing the flow. If the separation plane is sufficiently large, it is then possible to remove half of the wing and to replace it by the pressure leads and support for the remaining half. Figure 2 shows the airfoil and separation plane set up in the tunnel. The airfoil was mounted on a turntable fitted with an extension outside of the tunnel test section for changing the angle of attack.

Pressures at the various orifices were indicated as heads of alcohol by two liquid multiple manometers. Rubber tubes connected the manometers to the small brass nipples extending from the wing. All of the upper surface orifices were connected to one manometer, and those of the lower surface to the other. Two tubes of each manometer were connected to a static pressure plate in the wall of the tunnel test section just ahead of the model, for obtaining a reference pressure. Figure 3 shows the manometers, the rubber tubes leading from them to the wing, and the model support extension for changing the angle of attack. The model and separation plane, as well as the fairing enclosing the pressure tubes in the tunnel, are also partially shown.

Photographic records of the various pressures were obtained by placing a sheet of photostat paper behind the glass tubes of each manometer and flashing a 25-watt light located about 5 feet in front of each. The pressures on the upper and lower surface of the airfoil for one angle of attack are shown in the sample record, Figure 4.

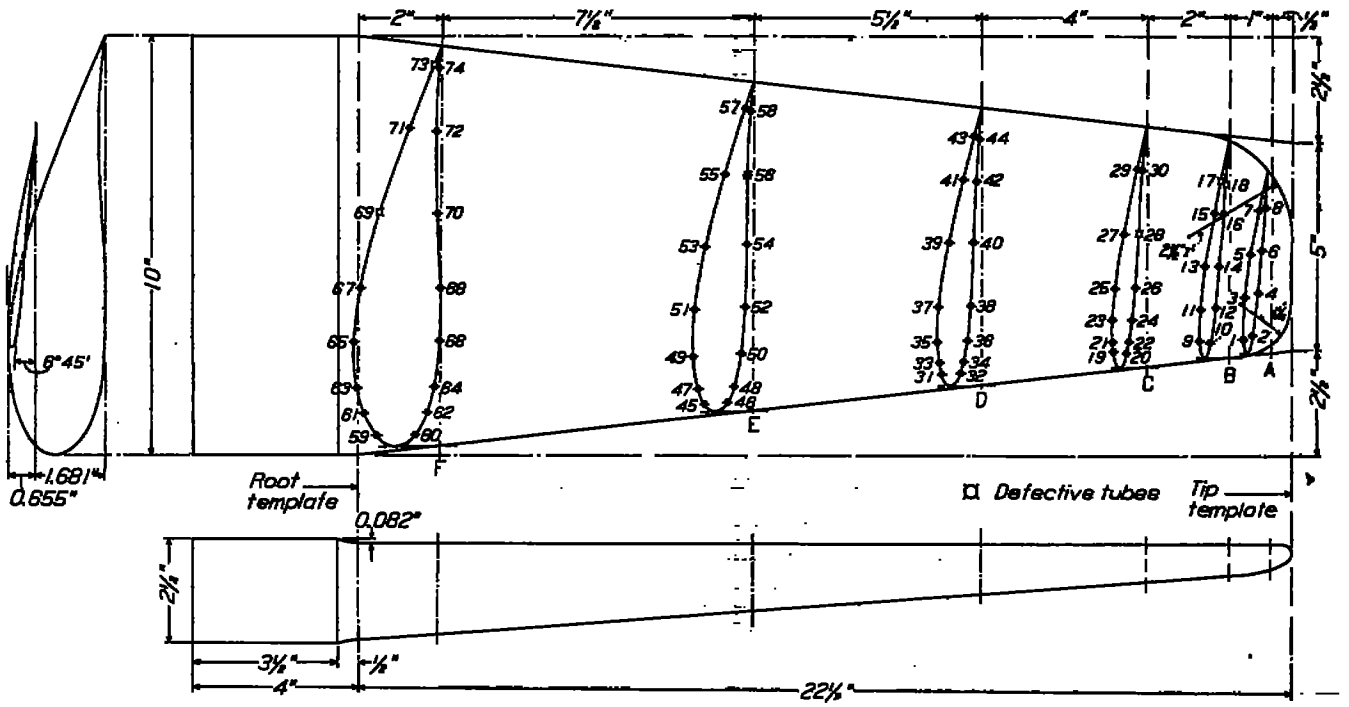

FIGURE 1.—N. A. C. A. 81-J pressure distribution wing

TESTS

A few preliminary tests were made for purposes of adjustment and calibration. Since the air flow is somewhat retarded close to the surface of the separation plane, it was necessary to compensate for the decrease in velocity. This was accomplished by inclining the leading edge of the plane, which consisted of a hinged flap 5½ inches wide, until vertical velocity surveys made about 1 foot upstream from the model showed a satisfactory dynamic pressure distribution.

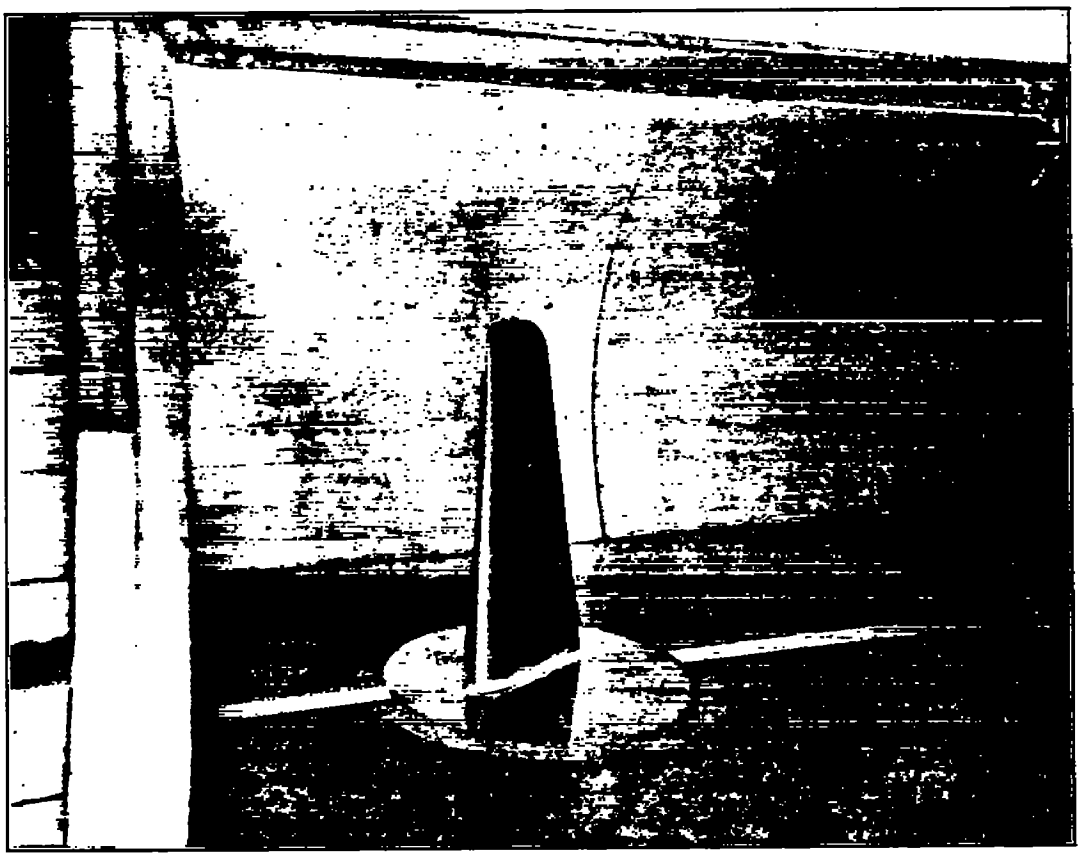

FIGURE 2.—Airfoil and separation plane set-up in tunnel

The model was set at the angle of attack of zero lift for these surveys, and it is fairly certain that the flow past the tunnel test section would be practically the same with the model removed. A Pitot-static tube installed permanently in the tunnel, sufficiently far upstream from the model to be unaffected by it, was then calibrated against the integrated mean of the final survey (fig. 5), and used as a dynamic pressure reference.

In testing the wing, it was necessary to set accurately the initial angle of attack. This was done by means of an optical system, which included a light source, lens, and indicating screen mounted on the side of the tunnel test chamber, and a mirror placed on the model parallel to the chord of the root section. The index on the wing support extension was then set according to the zero setting of this system.

The test procedure consisted of setting the angle of attack of the wing by means of the two handles and index on the wing support extension (see fig. 3), and allowing about a minute for the manometers to reach equilibrium. Then the photostat paper was placed in each manometer and an exposure of about one second was made. The paper was then removed, and the process repeated for another angle of attack. Check records taken during the tests indicated an accuracy in measured pressure heads of within ±1.0 per cent.

The pressure distribution tests were made at angles of attack ranging from −11° to +90°. Throughout the tests the dynamic pressure was maintained constant at 6.47 pounds per square foot, corresponding to an air speed of about 50.3 m. p. h. The average Reynolds Number was 283,000 with the mean wing chord as the characteristic length.

RESULTS

The results are given in Tables III, IV, and V in terms of the coefficients of relative load, normal force, and pitching moment, for each test section. Table VI gives the coefficients of normal force, lateral center of pressure, bending moment, pitching moment, and longitudinal center of pressure, for the whole wing. The results are also presented in graphical form as follows:

Figure 7. Section normal load coefficient versus angle of attack, K versus α.

Figures 8a and 8b. Span load diagrams, K versus span.

Figures 9 to 15. Isometric total normal pressure diagrams, including *C. P.* loci.

Figure 16. Angles of zero C_{NF} for each test section.

Figure 17. Total normal force coefficient versus angle of attack, C_{NF} versus α.

The results are presented without corrections for tunnel wall and blocking effects which have not been evaluated up to the present for set-ups of this type, a cross-sectional diagram of which is given in Figure 6. However, these tests are comparable with tests of the earlier wings given in Reference 1. When interpreting the results in terms of the full scale airplane, consideration should also be given to the low Reynolds Number at which the tests were conducted.

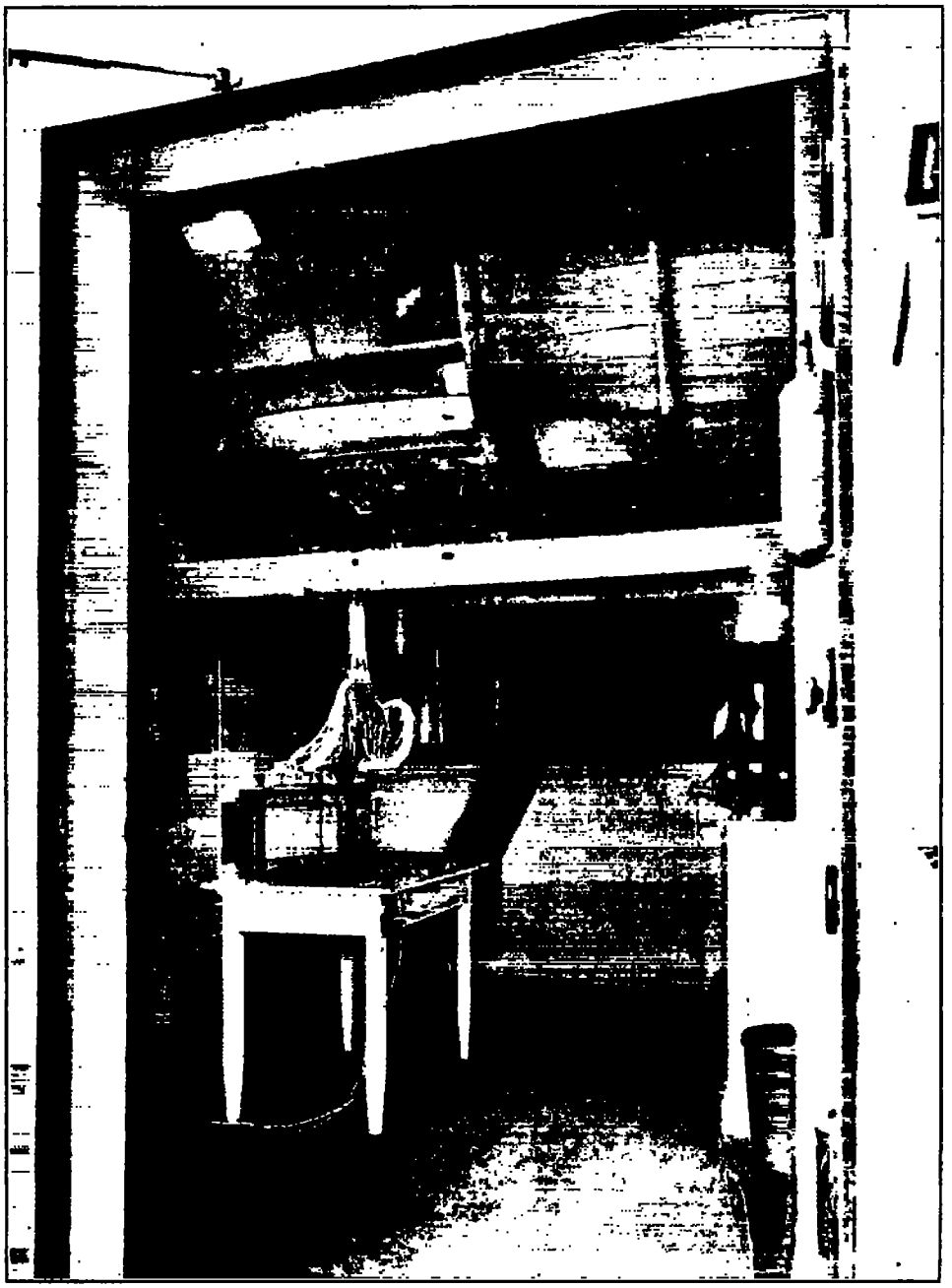

FIGURE 3.—Manometer installation

Figure 18. Total lateral center of pressure coefficient versus angle of attack, C_{py} versus α.

Figure 19. Total bending moment coefficient versus angle of attack, C_L' versus α.

Figure 20. Total pitching moment coefficient versus angle of attack, C_M versus α.

Figure 21. Total longitudinal center of pressure coefficient versus angle of attack, C_p versus α.

The results as presented in graphic and tabular form may be relied upon to within ± 3 per cent.

Actual pressure diagrams at each angle of attack were obtained by scaling values of the liquid heights from the

photostats, plotting them on cross-section paper at their correct positions along the chords of the airfoil, and fairing a closed curve through the points. These diagrams were then integrated for area, and for moments about the leading edge for each section. Check integrations gave an accuracy of within ±2 per cent for final values of areas and moments.

that used in a previous report (Reference 1), and was obtained as follows:

$$K = C_{NF} \times \frac{\text{chord}}{\text{semispan}}$$

This form of coefficient was necessitated by the fact that C_{NF} does not represent the loads along the span on account of the changing chord of the wing.

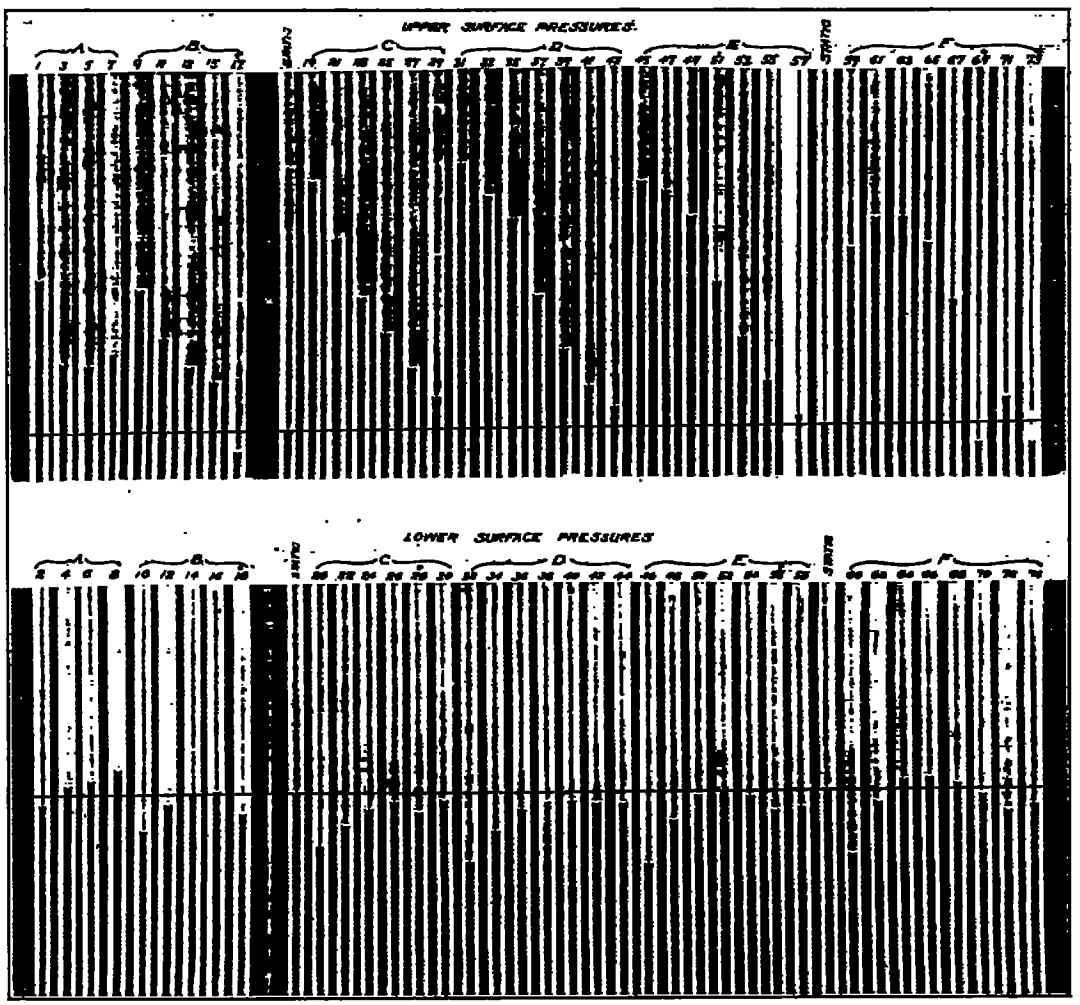

FIGURE 4.—Sample pressure record—N. A. C. A. 81-J airfoil $\alpha = +3°$

Values of normal force coefficients, C_{NF}, for the various sections were calculated from the faired diagrams as follows:

$$C_{NF} = \frac{A}{q\ c}$$

where

A = integrated area of the pressure diagram,
c = length of the diagram,
q = dynamic pressure, expressed as a head of the manometer liquid.

The relative normal loadings at the various test sections, expressed in nondimensional form, are given in Figures 7, 8a, and 8b. The coefficient is the same as

The distribution of the total pressures acting normal to the chord at each section for a given angle of attack has been plotted on isometric plan views of the wing, Figures 9 to 15. Lifting pressures are plotted upward and a pressure scale in terms of "q" is included on each figure. These diagrams also contain curves of centers of pressure along the span.

Values of total C_{NF} have been plotted for each angle of attack as shown in Figure 17. These total coefficients were obtained as follows:

$$C_{NF} = \frac{A'}{q\frac{S}{2}}$$

where

A' = area of the semispan load diagram. (The integrated area of each section load was plotted versus semispan, and the final curves integrated for total area),

S = total area of the wing,

q = dynamic pressure expressed as a head of the manometer liquid.

The lateral *C. P.*, Figure 18, was obtained by plotting areas of the section pressure diagrams versus

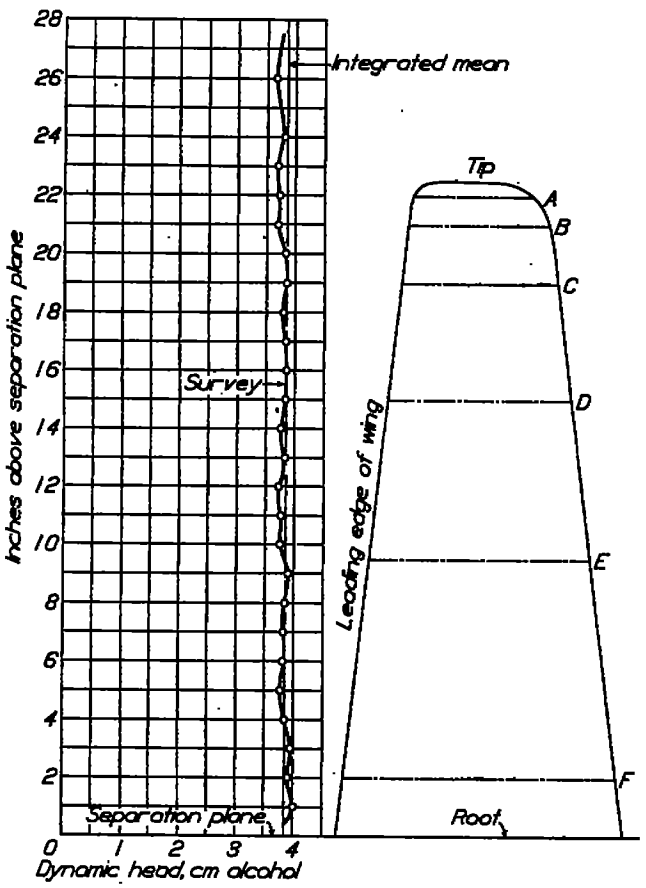

FIGURE 5.—Dynamic pressure survey (final)

semispan, integrating for area and for moments about the root, and then dividing the moment by the area. These values are given in per cent semispan from the wing root.

The bending moments about the wing root, Figure 19, have been calculated in coefficient form by the product of the total normal force coefficient and the lateral center of pressure coefficient as follows:

$$C_L' = C_{NF} \times C_{pr},$$

from which

$$C_L' = \frac{A'}{q\,\frac{S}{2}} \times \frac{L'}{A'\,\frac{b}{2}},$$

or

$$C_L' = \frac{4\,L'}{q\,b\,S},$$

where

L' = bending moment about the root,

b = span of the wing,

S = total area of the wing,

q = dynamic pressure,

all in consistent units.

Total pitching moment coefficients, Figure 20, were obtained from

$$C_M = \frac{A''}{q\,c\,\frac{S}{2}}$$

where

A'' = area of semispan moment diagram. (The integrated pitching moment about the leading edge of the root section extended was plotted for each section versus semispan, and the final curve integrated for total area.)

c = chord of root section,

S = total area of the wing,

q = dynamic pressure, expressed as a head of the manometer liquid.

The total longitudinal center of pressure coefficients, Figure 21, were obtained by dividing the total pitching moment coefficients C_M by the total normal force coefficient C_{NF}. Results are given in per cent root chord from the leading edge of the root section.

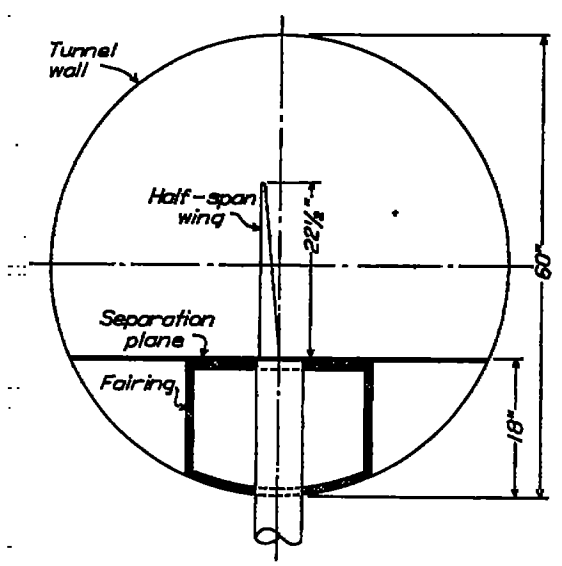

FIGURE 6.—Cross section of tunnel set-up

DISCUSSION

The loading on the tip section, "A," is relatively light as may be seen from Figure 7, while the section loading gradually increases from tip to root. The span load distribution, Figures 8a and 8b, is seen to approach the desired elliptical shape, which is also the condition for minimum induced drag of the wing. The actual load distribution for a full scale wing of this design may be obtained after determining the loadings at various points along the span by the following relation:

$$\text{Load per unit span} = K \times q \times \text{semispan} \qquad (1)$$

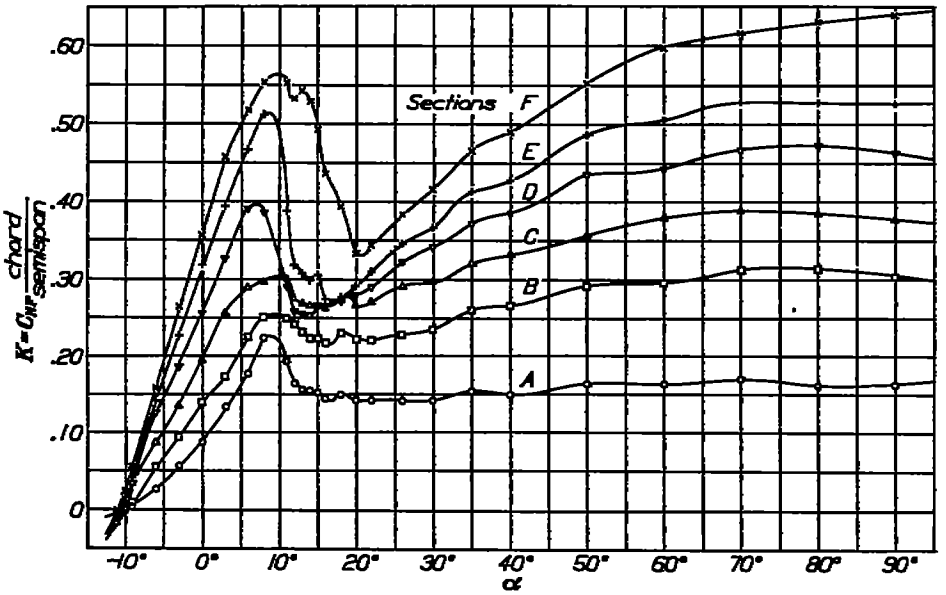

FIGURE 7.—Normal load coefficient (section) versus angle of attack

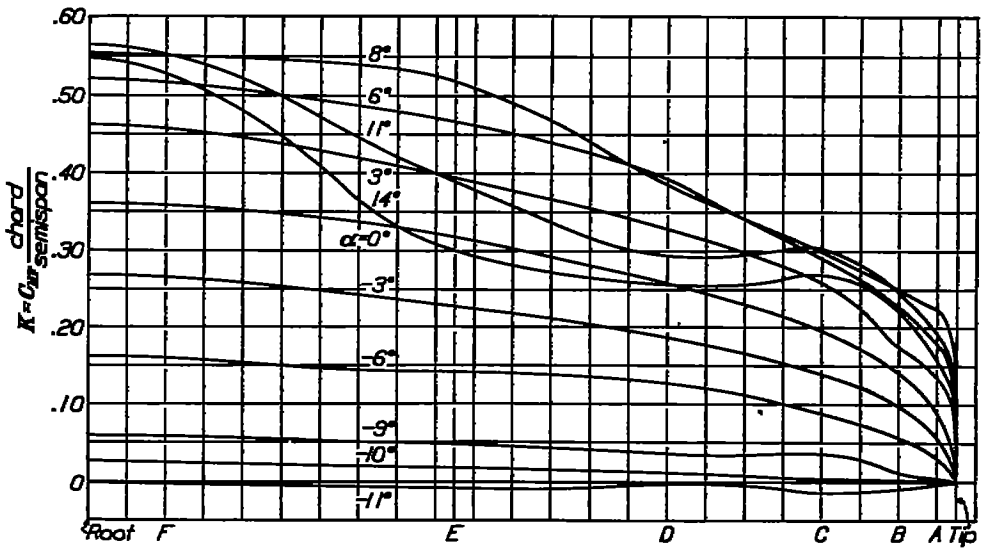

FIGURE 8a.—Semispan load diagram

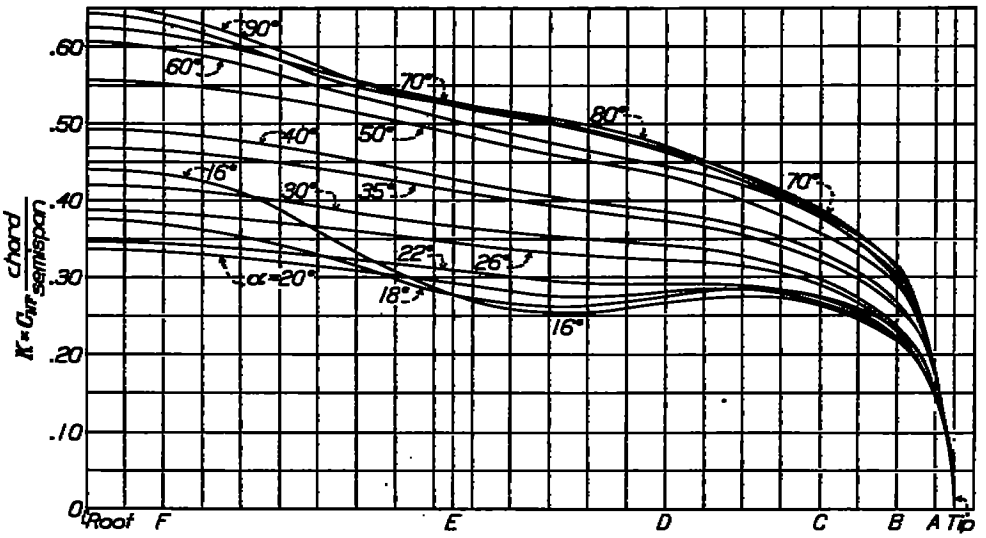

FIGURE 8b.—Semispan load diagram

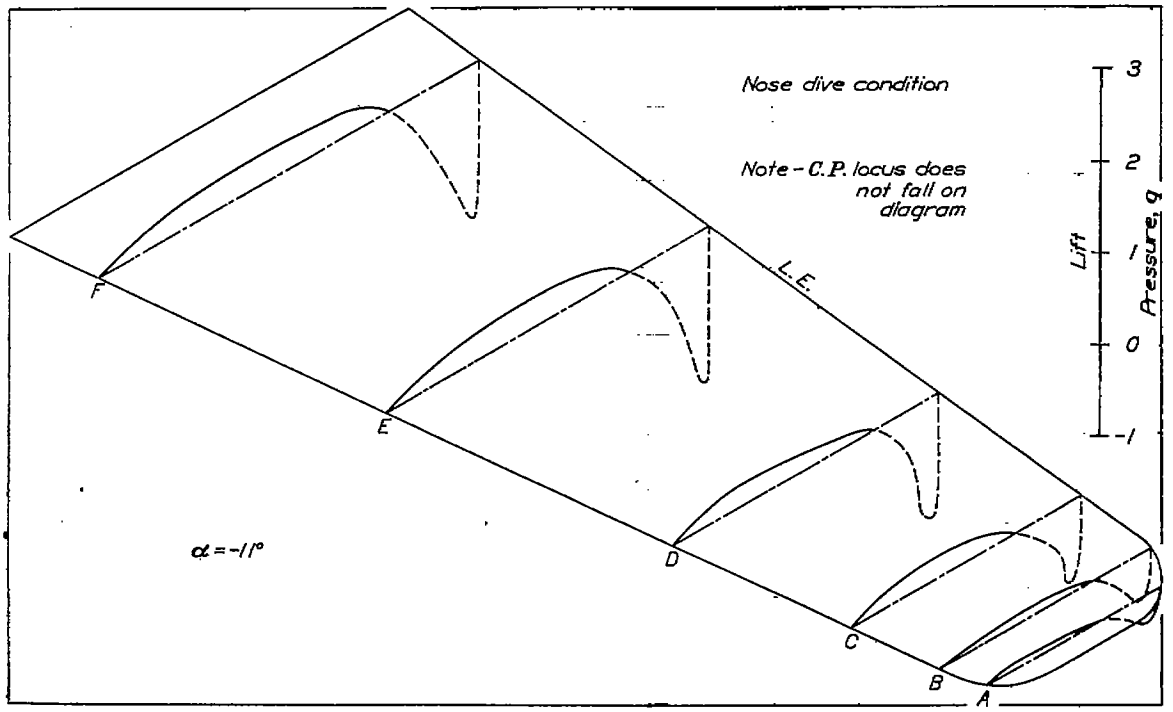

FIGURE 9.—Total normal pressure distribution

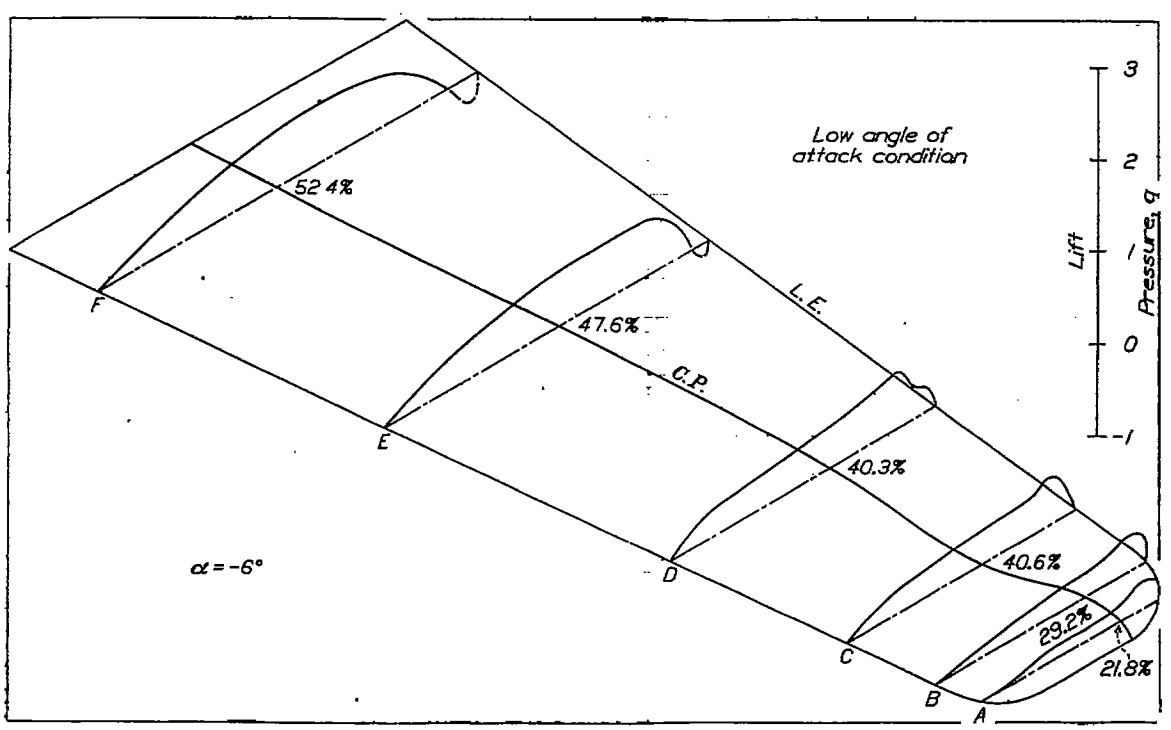

FIGURE 10.—Total normal pressure distribution

A few representative isometric pressure diagrams, presented in Figures 9 to 15, are of interest in that they show the distribution of the total pressures acting normal to the test section chords of the wing. The angles of attack below the stall, Figures 9, 10, and 11, were chosen so as to show the loadings for three standard design conditions, i. e., nose dive, low angle of attack, and high angle of attack. Figures 12 to 15 give a general idea of conditions above the stall up to 90°.

Since one of the objects to be attained with the new wing was that all sections along the span should reach zero lift simultaneously, reference to Figure 16 shows the degree to which this has been accomplished. The angle of zero lift of each section lies within ±0.4° of the angle of attack of zero lift for the whole wing. This may be considered to be a sufficiently close approximation to the above desired condition.

It can be seen, however (fig. 16), that an additional washin of about 0.8° would probably give still better results with this wing. The total washin would then be 7.55° at the tips, which is a fairly close check on the theoretical value of 7.75° as calculated by the method given in reference 4. It should be noted, however, that the span loading and bending moments might be changed appreciably from those shown in the low angle of attack range for the wing if the greater twist is used.

The normal force characteristics of the wing as a whole are given in Figure 17. A maximum value of C_{NF} of 1.33 was obtained at $\alpha=8.5°$. Since the coefficients of normal force and of lift for a given wing are practically of the same magnitude up to the angle of maximum lift, the value of $C_{NF}=1.33$ represents a relatively high lift coefficient for this wing. To determine the normal force NF, for a given wing, the following expression should be used:

$$NF=q\,S\,C_{NF} \tag{2}$$

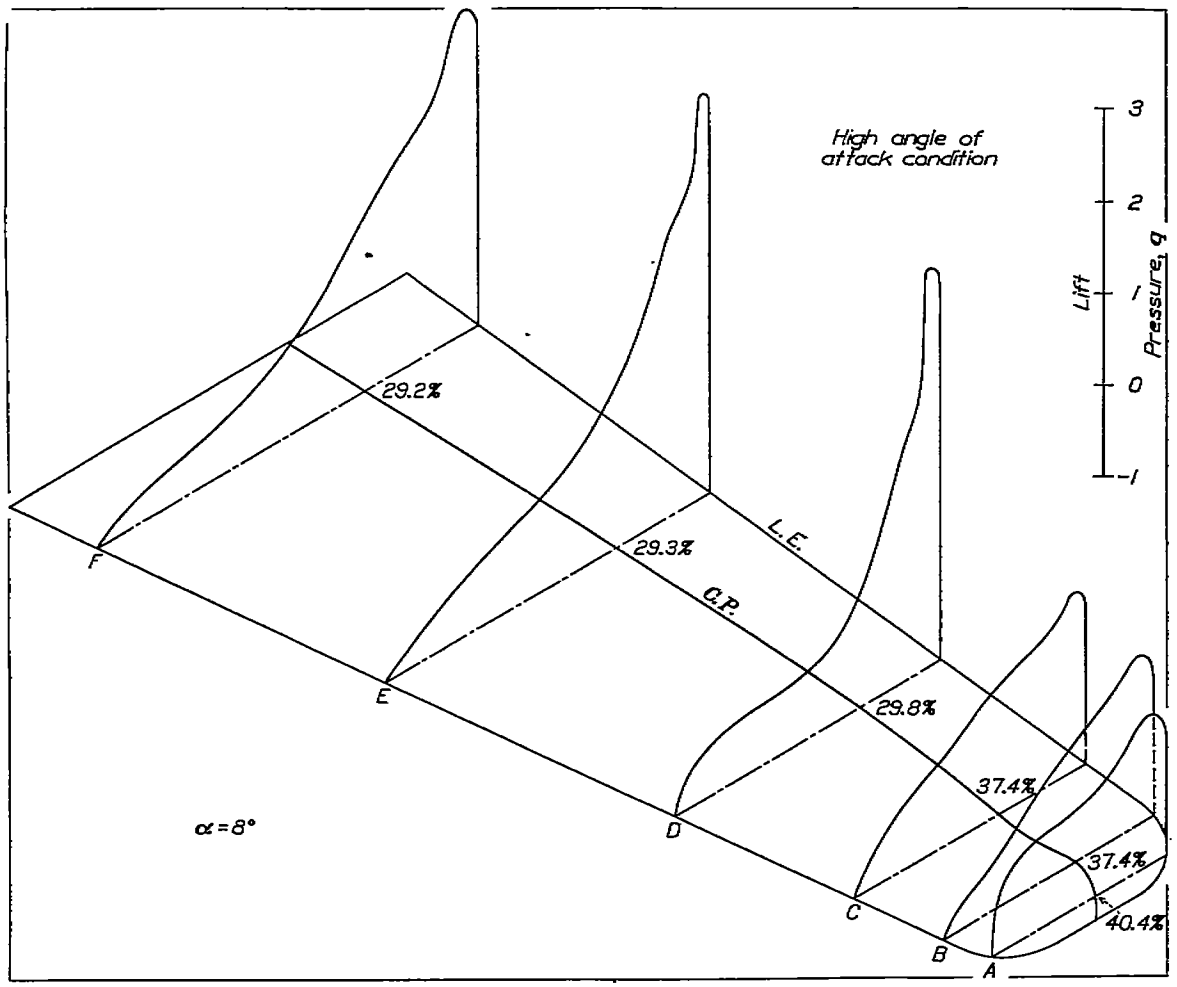

FIGURE 11.—Total normal pressure distribution

The lateral $C.\ P.$, Figure 18, lies at about 43 per cent of the semispan from the wing root up to the angle of maximum lift, $\alpha=8.5°$. It then moves slightly toward the root and then outward to an average of about 45 per cent semispan for angles of attack ranging from 20° to 90°.

The bending moments about the wing root in coefficient form shown in Figure 19 apply only to a full cantilever wing. To evaluate the bending moments, L', about the root for the full scale wing, use should be made of the following:

$$L'=\frac{q\,S\,b\,C_L'}{4} \tag{3}$$

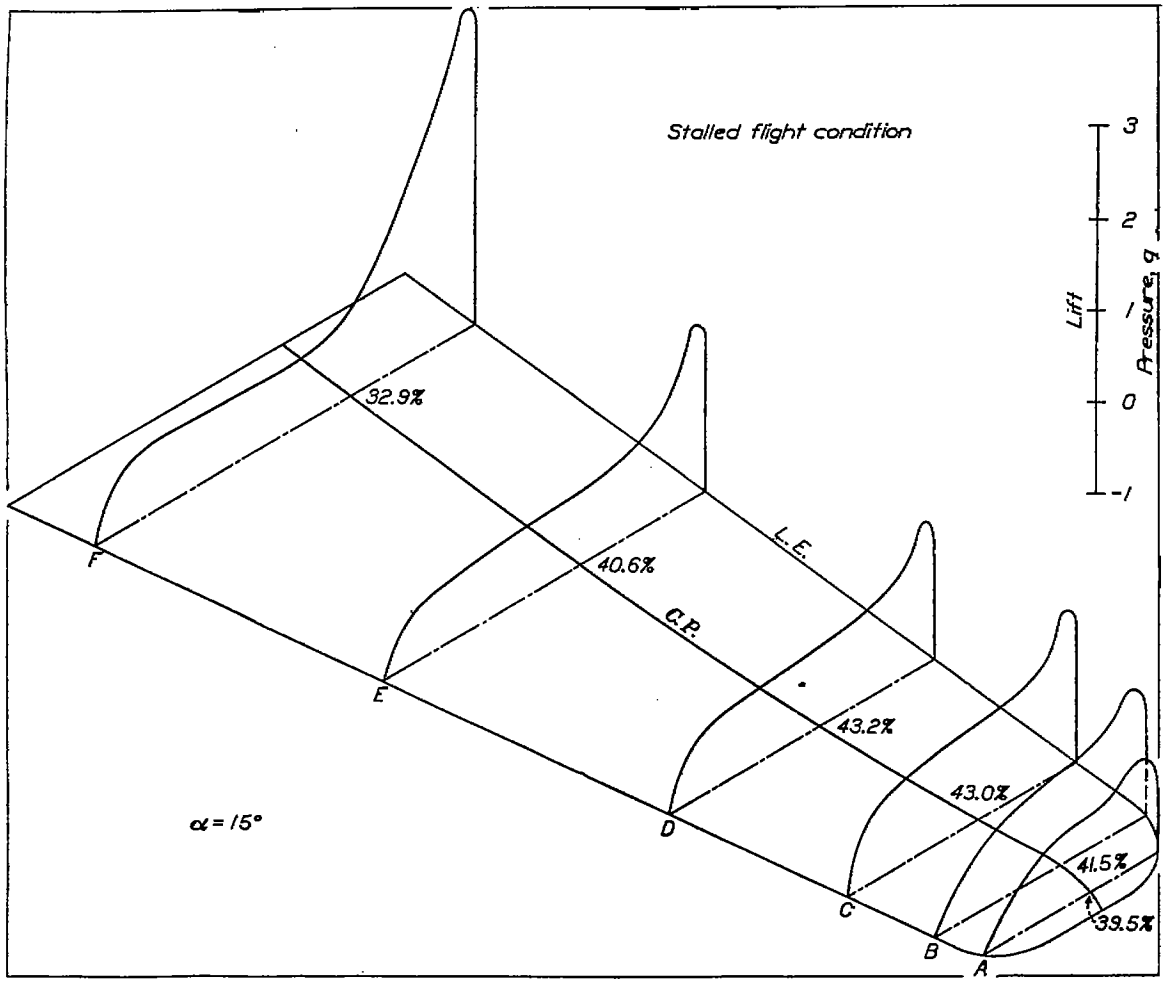

FIGURE 12.—Total normal pressure distribution

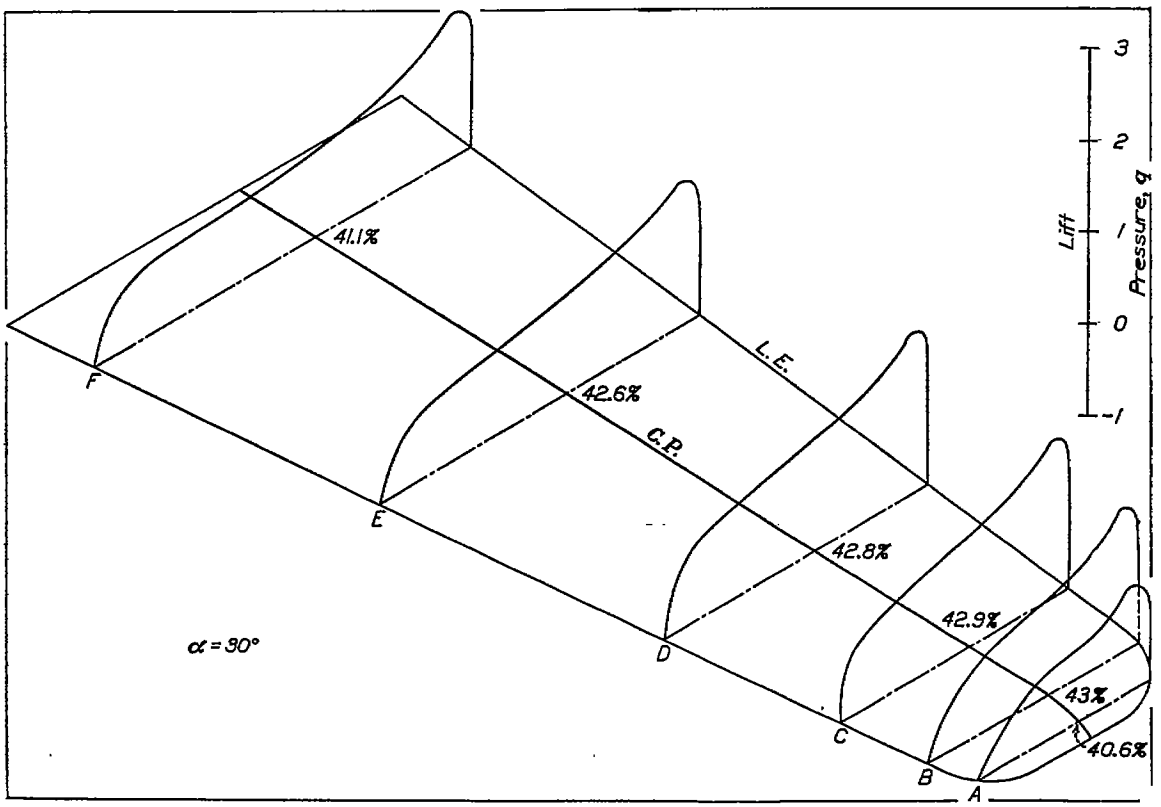

FIGURE 13.—Total normal pressure distribution

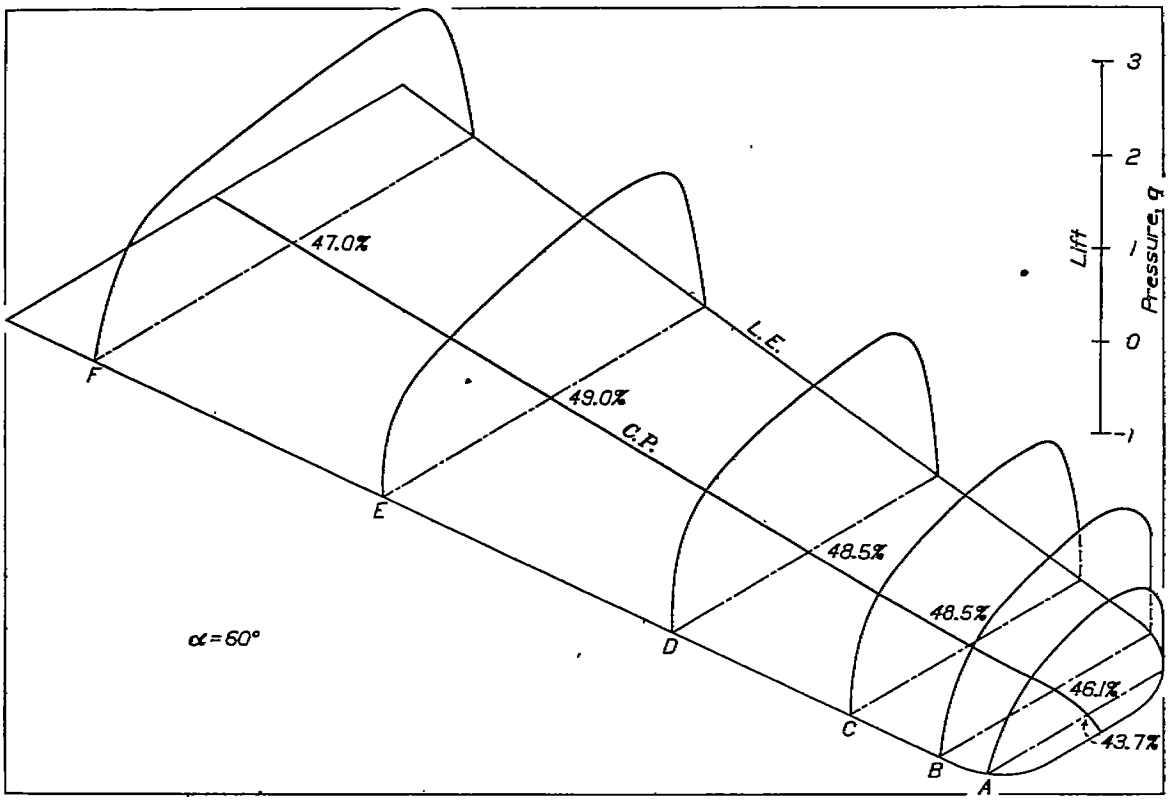

FIGURE 14.—Total normal pressure distribution

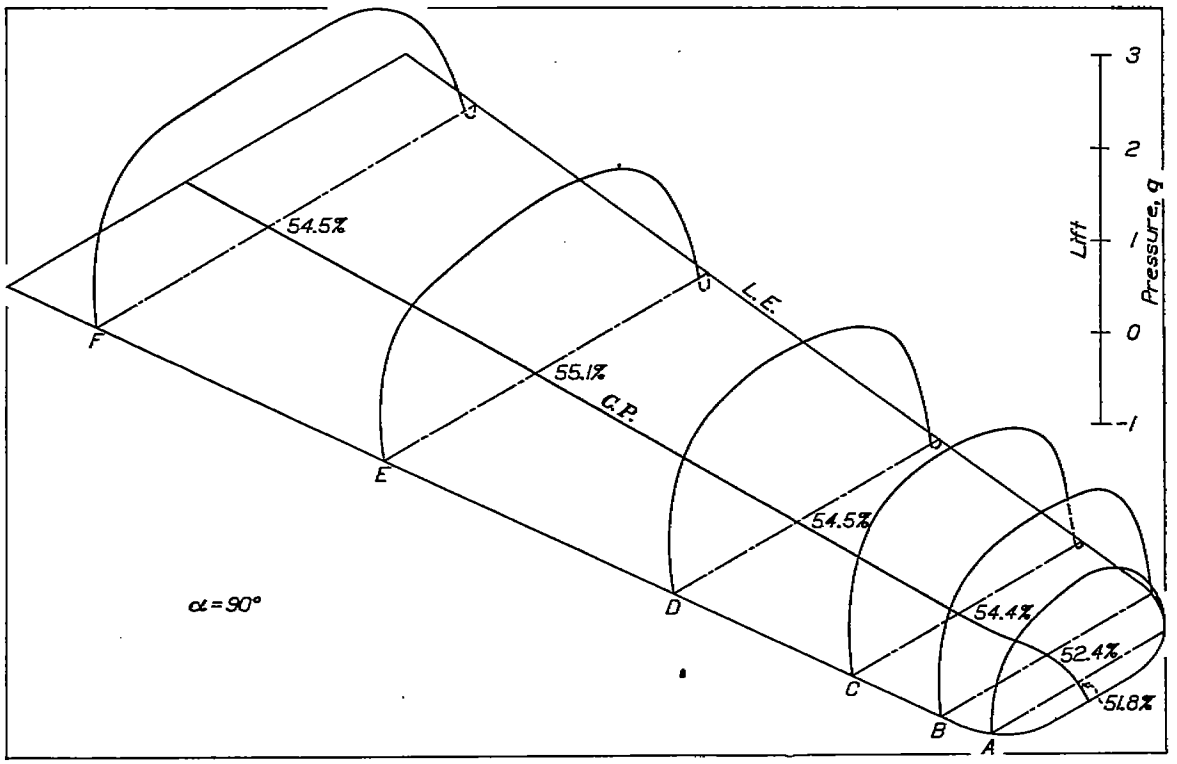

FIGURE 15.—Total normal pressure distribution

The total pitching moment coefficients, Figure 20, and longitudinal *C. P.* travel, Figure 21, are included to facilitate determination of the longitudinal stability and balance characteristics of the wing. The total

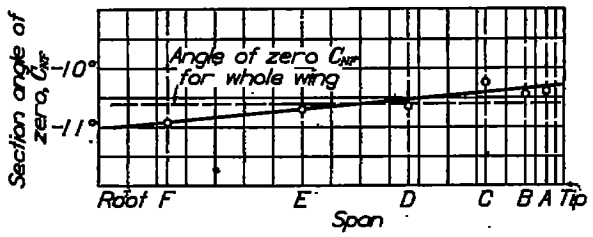

FIGURE 16.—Angle of zero C_{NF} for each section

pitching moment about the leading edge of the root section extended may be obtained from the following:

$$M = q\ c\ S\ C_M \tag{4}$$

CONCLUSIONS

1. The span load distribution over the N. A. C. A. 81–J wing is approximately of elliptical shape for the

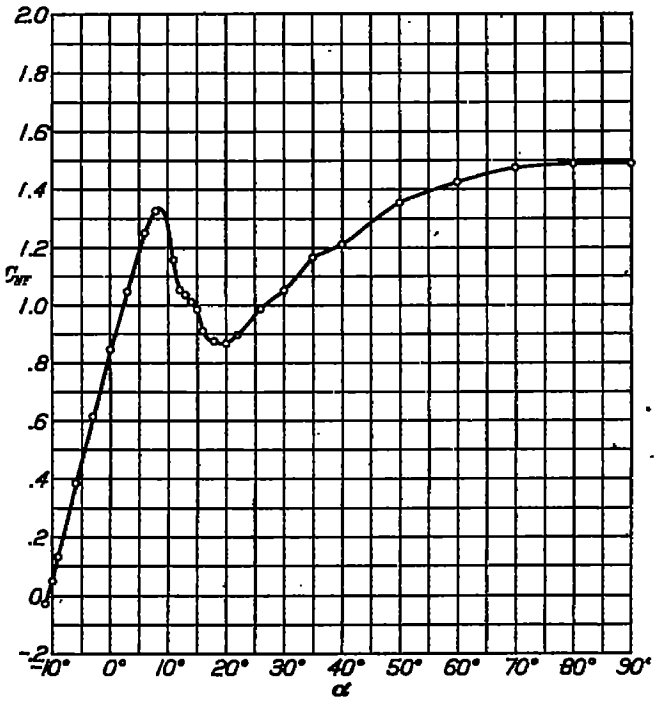

FIGURE 17.—Normal force coefficient (total) versus angle of attack

normal flying range, giving rise to relatively small bending moments about the wing root.

2. All sections along the span of the wing reach zero lift within ±0.4° of the angle of attack of zero lift for the whole wing, resulting in small loads on the leading edge of the wing for the nose dive condition of flight.

3. An additional washin of 0.8° at the tip would probably further improve the aerodynamic properties of the wing in the region of zero lift.

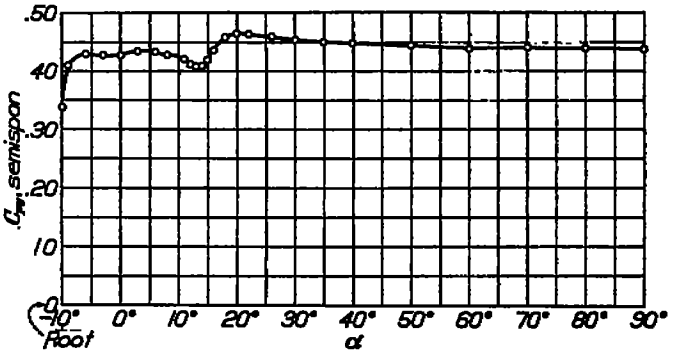

FIGURE 18.—Lateral center of pressure coefficient (total) versus angle of attack

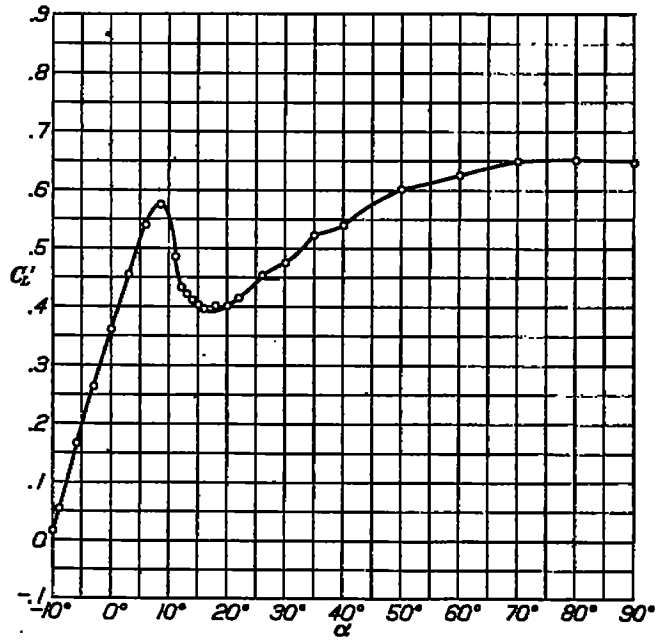

FIGURE 19.—Bending moment coefficient versus angle of attack

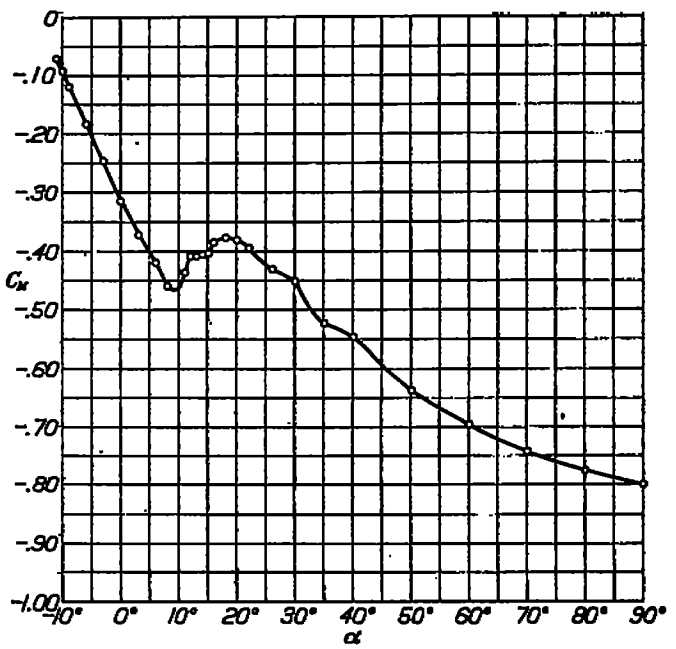

FIGURE 20.—Pitching moment coefficient (total) versus angle of attack. Moments taken about L. E. of root section extended

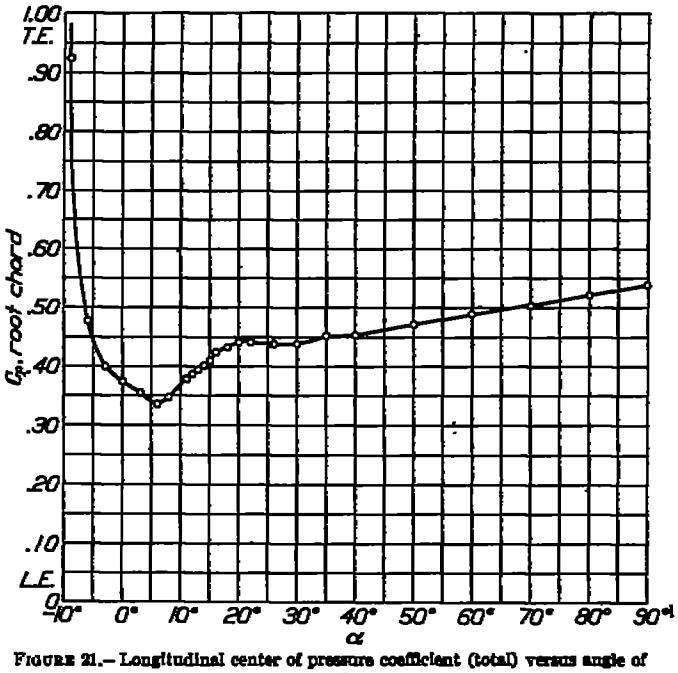

FIGURE 21.—Longitudinal center of pressure coefficient (total) versus angle of attack

4. A relatively high value of maximum lift coefficient, 1.33, has been attained with the wing.

LANGLEY MEMORIAL AERONAUTICAL LABORATORY,
NATIONAL ADVISORY COMMITTEE FOR AERONAUTICS,
LANGLEY FIELD, VA., *May 21, 1930.*

REFERENCES

Reference 1. Reid, Elliott G.: Pressure Distribution over Thick Tapered Airfoils: N. A. C. A. 81, U. S. A. 27 C modified, and U. S. A. 35. N. A. C. A. Technical Report No. 229. 1926.

Reference 2. Blumenthal, Otto: Pressure Distribution on Joukowski Wings, and
Trefftz, E.: Graphic Construction of Joukowski Wings. N. A. C. A. Technical Memorandum No. 336. 1925.

Reference 3. Reid, Elliott G.: Standardization Tests of N. A. C. A. No. 1 Wind Tunnel. N. A. C. A. Technical Report No. 195. 1924.

Reference 4. Munk, Max M.: The Determination of the Angles of Attack of Zero Lift and of Zero Moment, Based on Munk's Integrals. N. A. C. A. Technical Note No. 122. 1922.

Reference 5. Knight, M., and Loeser, O.: Pressure Distribution over a Rectangular Monoplane Wing Model up to 90° Angle of Attack. N. A. C. A. Technical Report No. 288. 1928.

TABLE I

ORDINATES

N. A. C. A. 81–J twisted and tapered monoplane wing

[The maximum ordinates of all sections lie in a horizontal plane when the root chord line is horizontal. Ordinates and stations in per cent of chord.]

Root section			Tip section	
Stations	Upper	Lower	Upper	Lower
0.0	12.25	12.25	3.06	3.06
1.25	15.76	8.00	3.94	2.00
2.50	17.10	6.75	4.28	1.68
5.00	18.95	4.95	4.74	1.24
7.50	20.25	3.65	5.06	0.91
10.00	21.25	2.70	5.31	0.68
12.50	21.94	1.96	5.49	0.50
15.00	22.45	1.40	5.61	0.35
17.50	22.83	0.99	5.72	0.25
20.00	23.15	0.68	5.79	0.17
22.50	23.30	0.44	5.83	0.11
25.00	23.36	0.29	5.84	0.07
30.00	23.07	0.08	5.76	0.02
35.00	22.45	0.00	5.61	0.00
40.00	21.62	0.05	5.41	0.01
45.00	20.56	0.20	5.16	0.05
50.00	19.25	0.45	4.81	0.11
55.00	17.80	0.70	4.45	0.17
60.00	16.20	0.94	4.05	0.23
65.00	14.45	1.16	3.61	0.29
70.00	12.61	1.36	3.15	0.34
75.00	10.70	1.49	2.67	0.37
80.00	8.68	1.50	2.17	0.37
85.00	6.59	1.38	1.65	0.34
90.00	4.45	1.00	1.11	0.25
95.00	2.30	0.52	0.58	0.13
100.00	0	0	0	0

TABLE II

Orifice locations—N. A. C. A. 81–J pressure distribution wing

A		B		C		D		E		F	
Orifice	*	Orifice	*	Orifice	*	Orifice	*	Orifice	*	Orifice	*
1	3.2	9	4.0	19	3.7	31	2.7	45	2.0	59	2.6
2	4.1	10	8.6	20	3.3	32	2.8	46	2.4	60	2.6
3	13.3	11	11.6	21	6.0	33	5.5	47	5.7	61	7.7
4	14.2	12	11.8	22	6.0	34	5.5	48	6.2	62	7.8
5	22.5	13	21.8	23	11.3	35	10.4	49	13.3	63	12.6
6	24.4	14	21.8	24	11.2	36	10.6	50	14.0	64	12.9
7	33.7	15	34.4	25	18.7	37	18.8	51	24.6	65	24.6
8	34.4	16	34.3	26	18.8	38	18.8	52	25.0	66	25.0
		17	42.1	27	31.5	39	34.0	53	39.6	67	37.6
		18	41.4	28	31.7	40	33.8	54	40.0	68	37.7
				29	47.0	41	49.0	55	56.8	69	55.5
				30	46.8	42	48.4	56	56.5	70	55.4
						43	59.0	57	72.2	71	75.6
						44	58.5	58	71.5	72	75.0
										73	90.7
										74	90.0

*Per cent of root chord from L. E. of each section.

TABLE III

Section relative load coefficients,

$$K = C_{NF} \times \frac{\text{Chord}}{\text{Semispan}}$$

N. A. C. A. 81–J tapered wing

α	A	B	C	D	E	F
−11°	−0.0035	−0.0081	−0.0157	−0.0041	−0.0087	−0.0011
−10°	+.0018	+.0035	+.0041	+.0116	+.0186	+.0260
−9°	.0047	.0104	.0365	.0372	.0470	.0590
−6°	.0296	.0575	.0999	.128	.142	.161
−3°	.0575	.0970	.137	.188	.228	.265
0°	.0895	.141	.195	.256	.319	.357
+3°	.135	.175	.238	.327	.394	.456
6°	.179	.226	.289	.391	.466	.516
8°	.224	.251	.297	.387	.511	.552
11°	.194	.249	.300	.292	.388	.552
12°	.166	.242	.275	.260	.319	.532
13°	.158	.231	.269	.256	.309	.542
14°	.157	.224	.267	.256	.300	.528
15°	.154	.224	.258	.265	.306	.493
16°	.146	.218	.253	.267	.275	.426
18°	.151	.232	.275	.275	.277	.369
20°	.143	.232	.267	.281	.291	.334
22°	.144	.223	.271	.290	.310	.344
25°	.143	.229	.290	.322	.345	.383
30°	.143	.235	.296	.341	.366	.416
35°	.156	.261	.320	.372	.412	.465
40°	.152	.267	.331	.385	.427	.489
50°	.157	.291	.356	.434	.486	.552
60°	.166	.297	.379	.442	.504	.598
70°	.172	.313	.388	.466	.527	.616
80°	.164	.315	.384	.471	.525	.631
90°	.165	.306	.377	.463	.525	.641

TABLE IV

Section normal force

coefficients. C_{NF}

N. A. C. A. 81–J tapered wing

α	A	B	C	D	E	F
−11°	−0.0182	−0.0348	−0.0654	−0.0136	−0.0248	−0.0027
−10°	+.0091	+.0149	+.0157	+.0390	+.0539	+.0600
−9°	.0242	.0447	.141	.125	.134	.139
−6°	.154	.246	.347	.429	.407	.378
−3°	.299	.415	.536	.632	.550	.622
0°	.466	.602	.751	.861	.908	.837
+3°	.705	.751	.992	1.097	1.121	1.007
6°	.932	.967	1.114	1.312	1.326	1.210
8°	1.165	1.076	1.143	1.300	1.454	1.294
11°	1.001	1.064	1.154	.981	1.106	1.295
12°	.865	1.034	1.060	.872	.909	1.250
13°	.823	.989	1.036	.862	.881	1.271
14°	.820	.989	1.028	.860	.855	1.240
15°	.802	.959	1.032	.891	.872	1.158
16°	.762	.934	1.013	.897	.784	1.027
18°	.786	.994	1.060	.924	.788	.865
20°	.747	.966	1.029	.944	.827	.784
22°	.750	.951	1.046	.975	.884	.808
25°	.743	.981	1.119	1.060	.984	.898
30°	.743	1.008	1.141	1.143	1.044	.975
35°	.814	1.118	1.233	1.250	1.173	1.091
40°	.790	1.142	1.272	1.293	1.217	1.149
50°	.866	1.244	1.370	1.456	1.385	1.296
60°	.865	1.271	1.460	1.501	1.437	1.406
70°	.895	1.339	1.495	1.565	1.500	1.448
80°	.853	1.350	1.480	1.590	1.496	1.431
90°	.859	1.318	1.454	1.556	1.495	1.504

TABLE V

Section pitching moment

coefficients C_M

[About leading edge of root section extended]

N. A. C. A. 81–J tapered wing

α	A	B	C	D	E	F
−11°	−0.017	−0.047	−0.061	−0.086	−0.095	−0.113
−10°	−.014	−.055	−.075	−.105	−.114	−.127
−9°	−.039	−.061	−.119	−.119	−.142	−.145
−6°	−.084	−.072	−.133	−.173	−.193	−.196
−3°	−.087	−.119	−.172	−.214	−.236	−.258
0°	−.157	−.176	−.230	−.273	−.302	−.301
+3°	−.255	−.246	−.286	−.333	−.343	−.324
6°	−.381	−.302	−.329	−.359	−.382	−.364
8°	−.470	−.402	−.427	−.387	−.426	−.378
11°	−.408	−.425	−.481	−.411	−.399	−.378
12°	−.356	−.446	−.456	−.382	−.372	−.369
13°	−.338	−.413	−.447	−.366	−.367	−.398
14°	−.319	−.398	−.438	−.362	−.353	−.413
15°	−.316	−.393	−.443	−.381	−.354	−.382
16°	−.316	−.387	−.419	−.381	−.334	−.378
18°	−.308	−.416	−.434	−.389	−.340	−.326
20°	−.291	−.391	−.421	−.410	−.356	−.324
23°	−.305	−.391	−.431	−.410	−.384	−.336
26°	−.297	−.406	−.466	−.454	−.418	−.375
30°	−.311	−.438	−.488	−.488	−.444	−.401
35°	−.330	−.476	−.536	−.541	−.531	−.471
40°	−.329	−.491	−.566	−.576	−.538	−.496
50°	−.364	−.557	−.646	−.673	−.642	−.588
60°	−.378	−.587	−.706	−.726	−.704	−.663
70°	−.431	−.644	−.726	−.781	−.759	−.720
80°	−.431	−.659	−.753	−.829	−.756	−.755
90°	−.445	−.601	−.790	−.845	−.835	−.821

TABLE VI

Total wing coefficients

N. A. C. A. 81–J tapered wing

α	C_{NF}	C_{NF} % $\frac{b}{2}$	C_L'	C_M	C_p % Root c
−11°	−0.021	75.30	−0.0188	−0.071	−338
−10°	+.050	33.60	+.0108	−.092	+164
−9°	.130	40.80	.0641	−.120	92.3
−6°	.387	42.86	.166	−.184	47.5
−3°	.614	42.60	.262	−.246	40.0
0°	.845	42.52	.360	−.316	37.4
+3°	1.049	43.31	.454	−.372	35.5
6°	1.250	43.02	.539	−.420	33.6
9°	1.323	42.31	.574	−.460	34.7
11°	1.187	41.81	.454	−.436	37.7
12°	1.051	41.00	.432	−.408	38.8
13°	1.038	40.68	.420	−.408	39.4
14°	1.010	40.60	.410	−.405	40.1
15°	.985	41.81	.408	−.403	40.9
16°	.909	43.38	.394	−.385	42.4
18°	.872	45.71	.398	−.377	43.2
20°	.884	46.30	.400	−.381	44.1
22°	.895	46.15	.413	−.396	44.1
25°	.937	45.75	.462	−.432	43.8
30°	1.049	45.21	.474	−.459	43.8
35°	1.161	44.85	.531	−.525	45.1
40°	1.209	44.51	.538	−.547	45.3
50°	1.351	44.40	.600	−.639	47.2
60°	1.422	43.78	.624	−.697	49.9
70°	1.472	43.90	.648	−.743	50.4
80°	1.486	43.79	.650	−.775	52.1
90°	1.488	43.56	.6474	−.801	53.9